13th World Conference on Earthquake Engineering
Vancouver, B.C., Canada
August 1-6, 2004
Paper No. 657

SIZE AND SHAPE EFFECT ON FRP CONFINEMENTS FOR RECTANGULAR CONCRETE COLUMNS

Fang-Yao Yeh [1], Kuo-Chun Chang [2]

SUMMARY

The behavior of concrete columns of rectangular cross-sections confined with carbon fiber reinforced plastics (CFRP) is studied using the nonlinear finite element method. In this paper, effects of column size (D), CFRP volumetric ratio (ρ_j), column side to corner radius ratio (D/r) and column side aspect ratio (B/D) are studied. The confined concrete nonlinear constitutive relation for unequal lateral confining stresses, multi-axial concrete failure criterion and stiffness reduction methodology after concrete cracking or crushing are adopted. First, the finite element model is verified by comparing the numerical solutions of confined concrete with experimental results. Then the effects of column size (D), CFRP volumetric ratio (ρ_j), column side to corner radius ratio (D/r) and column side aspect ratio (B/D) on the peak strength and ductility of the confined concrete are considered.

There are 28 rectangular section concrete column specimens in this paper. Dimension of the column side length (D) considered are 15cm, 30 cm and 45 cm. The CFRP volumetric ratio are 0.5% and 1.0%. The column side to corner radius ratio (D/r) are 5, 10 and 15. The column side aspect ratio (B/D) are 1.0, 1.5 and 2.0. It is found that the carbon fiber composite can significantly increase the compressive strength and ductility of concrete.

The test results and results of parametric study indicate that the column axial compressive strength and ductility increase with increasing CFRP volumetric ratio (ρ_j), but decrease with increasing column side to corner radius ratio (D/r) and increasing column side aspect ratio (B/D). For columns with the same corner radius (r) and CFRP volumetric ratio (ρ_j), the column axial compressive strength and ductility decrease with increasing column size (D) and column side to corner radius ratio (D/r).

INTRODUCTION

The merits of CFRP include anti-corrosion, lightweight, easy cutting and construction, as well as high strength and high elastic modulus. For these reasons, CFRP has been widely used in retrofitting and strengthening reinforced concrete structures, especially in regions under high seismic risk or high chloride corrosion. In the wake of recent earthquakes, such as 1994 Northridge Earthquake (U.S.A.), the 1995 Kobe Earthquake (Japan), and the 1999 Ji-Ji Earthquake (Taiwan), the use of CFRP composite material has become a popular alternative for seismic retrofit applications. Since Ji-Ji Earthquake, many research

[1] Ph.D., Department of Civil Engineering, National Taiwan University, Taipei, Taiwan
[2] Professor, Department of Civil Engineering, National Taiwan University, Taipei, Taiwan

projects have been carried out at NCREE (National Center for Research on Earthquake Engineering, Taiwan) and the results show that the FRP confined circular columns are more efficient in strength and ductility than square or rectangular columns. In order to understand the difference of failure mechanisms between FRP confined circular, square and rectangular columns, a nonlinear FEM model for FRP confined rectangular concrete columns has been developed in this paper.

NONLINEAR FINITE ELEMENT MODEL FOR FRP CONFINED RECTANGULAR CONCRETE COLUMNS

A FRP jacket, as opposed to a steel one that applies a constant confining pressure after yield, has an elastic behavior up to failure and therefore experts a continuously increasing confining action. The amount of this action depends on the lateral dilation of concrete, which in turn is affected by the confining pressure. As the compressive stress on the concrete increases, it begins to crack internally and expand laterally, resulting in an apparent increase in Poisson's ratio. The confinement effect is sensitive to the Poisson's ratio of concrete. The Poisson's ratio of concrete is not a constant. In this paper, the Poisson's ratio effect introduced by Kupfer et al.,1969 [1] is followed that allow one to implicitly account for the lateral dilation of concrete and its interaction with the FRP jacket. The Poisson's ratio can be expressed in the form:

$$\nu = \nu_0 \left[1.0 + 1.3763 \frac{\varepsilon_c}{\varepsilon_{co}} - 5.36 \left(\frac{\varepsilon_c}{\varepsilon_{co}} \right)^2 + 8.586 \left(\frac{\varepsilon_c}{\varepsilon_{co}} \right)^3 \right] \tag{1}$$

where ε_c = strain in direction of uniaxial loading; ε_{co} = compressive strain of unconfined concrete peak stress, respectively (generally $\varepsilon_{co} = 0.002$ can be assumed); $\nu_0 = 0.2$, the initial value of ν.

The nonlinear finite element model, including nonlinear constitutive relation for unequal lateral confining stresses, multi-axial stress state concrete failure criterion and stiffness reduction methodology after concrete cracking or crushing, is developed as follows.

Nonlinear constitutive relation for unequal lateral confining stresses

The starting point is a well-known stress-strain model for confined concrete by Mander et al., 1988 [2], which has been extensively tested against experimental data. The model is based on the formula:

$$f_c = \frac{f_{cc}^{'} xr}{r - 1 + x^r} \tag{2}$$

where

$$x = \frac{\varepsilon_c}{\varepsilon_{cc}};\ \varepsilon_{cc} = \varepsilon_{co} \left[1 + 5 \left(\frac{f_{cc}^{'}}{f_{co}^{'}} - 1 \right) \right] \tag{2a, b}$$

$$r = \frac{E_c}{E_c - E_{\sec}};\ E_{\sec} = \frac{f_{cc}^{'}}{\varepsilon_{cc}} \tag{2c, d}$$

where $f_{cc}^{'}$ = compressive strength of confined concrete; $f_{co}^{'}$ = compressive strength of unconfined concrete; ε_{cc} = compressive strain at confined peak stress $f_{cc}^{'}$; E_c = Young's modulus for concrete.

The general solution of the multi-axial failure criterion in terms of two lateral confining stresses is presented in Figure 1. The procedure to find the ultimate strength ratio is rather complex and an iterative procedure has to be used. In this paper an approximate equation proposed by Chang and Mander, 1994 [3] is used to represent the failure surface proposed by Mander et al., 1988 [2].

The equation is

$$K = \frac{f_{cc}^{'}}{f_{co}^{'}} = 1 + A\bar{x} \left(0.1 + \frac{0.9}{1 + B\bar{x}} \right) \tag{3}$$

with

$$\bar{x} = \frac{f_{l1}^{'} + f_{l2}^{'}}{2f_{co}^{'}} \tag{3a}$$

$$r = \frac{f_{l1}^{'}}{f_{l2}^{'}},\ f_{l2}^{'} \geq f_{l1}^{'} \tag{3b}$$

$$A = 6.8886 - (0.6069 + 17.275r)e^{-4.989r} \tag{3c}$$

$$B = \frac{4.5}{\frac{5}{A}(0.9849 - 0.6306e^{-3.8939r}) - 0.1} - 5 \tag{3d}$$

For a symmetric tri-axial state of stress $f_l = f_{l1} = f_{l2}$, the analytical confinement coefficient K given by Mander et al., 1988 [2] is:

$$K = -1.254 + 2.254\sqrt{1 + 7.94\bar{x}} - 2\bar{x} \tag{4}$$

Element stress-strain relationship

Concrete element is used for the three-dimensional modeling of solids with or without reinforcing rebars. The solid is capable of cracking in tension and crushing in compression. The stress-strain matrix [*D*] used for this element is defined as:

$$[D] = \left(1 - \sum_{i=1}^{N_r} V_i^R\right)[D_c] + \sum_{i=1}^{N_r} V_i^R [D_r]_i \tag{5}$$

where N_r = number of reinforcing materials; V_i^R = ratio of the volume of reinforcing material *i* to the total volume of the element; [D_c] = stress-strain matrix for concrete; and [D_r]$_i$ = stress-strain matrix for reinforcement *i*. Details of the matrix forms have been given in another paper by Chang and Yeh,2002 [4].

Multi-axial stress state concrete failure criterion

The failure criterion of concrete due to a multi-axial stress state can be expressed in the form

$$\frac{F}{f_{co}^{'}} - S \geq 0 \tag{6}$$

where F = a function of the principal stress state; S = failure surface; and $f_{co}^{'}$ = uniaxial compressive strength.

In the compression-compression-compression region ($0 \geq \sigma_1 \geq \sigma_2 \geq \sigma_3$), the failure criterion of Willam and Warnke, 1975 [5] is implemented. In this case, F takes the form

$$F = F_1 = \frac{1}{\sqrt{15}}\left[(\sigma_1 - \sigma_2)^2 + (\sigma_2 - \sigma_3)^2 + (\sigma_3 - \sigma_1)^2\right]^{1/2} \tag{7}$$

and S is defined as

$$S = S_1 = \frac{2r_2(r_2^2 - r_1^2)\cos\eta + r_2(2r_1 - r_2)\left[4(r_2^2 - r_1^2)\cos^2\eta + 5r_1^2 - 4r_1r_2\right]^{1/2}}{4(r_2^2 - r_1^2)\cos^2\eta + (r_2 - 2r_1)^2} \tag{7a}$$

The terms used to define S are:

$$\cos\eta = \frac{2\sigma_1 - \sigma_2 - \sigma_3}{\sqrt{2}\left[(\sigma_1 - \sigma_2)^2 + (\sigma_2 - \sigma_3)^2 + (\sigma_3 - \sigma_1)^2\right]^{1/2}} \tag{7b}$$

$$r_1 = a_0 + a_1\xi + a_2\xi^2 \tag{7c}$$

$$r_2 = b_0 + b_1\xi + b_2\xi^2 \tag{7d}$$

$$\xi = \frac{\sigma_h}{f_{co}^{'}},\quad \sigma_h = \frac{1}{3}(\sigma_1 + \sigma_2 + \sigma_3) \tag{7e, f}$$

Details of failure criteria under remainder stress states have been introduced in another paper by Chang and Yeh, 2002 [4].

Stiffness reduction methodology

In this paper, the finite element concrete model predicts either elastic behavior, cracking behavior or crushing behavior. If elastic behavior is predicted, the concrete is treated as a linear elastic material. If cracking or crushing behavior is predicted, the elastic, stress-strain matrix is adjusted as discussed below for one failure mode, and the remainders have been illustrated in another paper by Chang and Yeh [4].

The presence of a crack at an integration point is represented through modification of the stress-strain relation by introducing a plane of weakness in a direction normal to the crack face. Also, a shear transfer coefficient β_t is introduced which represents a shear strength reduction factor for those subsequent loads which induce sliding across the crack face. The stress-strain relations for a material that has cracked in one direction only become:

$$\left[D_c^{ck}\right]=\frac{E_c}{(1+\nu)(1-2\nu)}\begin{bmatrix} 0 & 0 & 0 & 0 & 0 & 0 \\ 0 & \frac{1-2\nu}{1-\nu} & \frac{\nu(1-2\nu)}{1-\nu} & 0 & 0 & 0 \\ 0 & \frac{\nu(1-2\nu)}{1-\nu} & \frac{1-2\nu}{1-\nu} & 0 & 0 & 0 \\ 0 & 0 & 0 & \beta_t\frac{(1-2\nu)}{2} & 0 & 0 \\ 0 & 0 & 0 & 0 & \frac{(1-2\nu)}{2} & 0 \\ 0 & 0 & 0 & 0 & 0 & \beta_t\frac{(1-2\nu)}{2} \end{bmatrix} \tag{8}$$

where the superscript ck signifies that the stress strain relations refer to a coordinate system parallel to principal stress directions with the x^{ck} axis perpendicular to the crack face.

If the material at an integration point fails in uniaxial, biaxial, or triaxial compression, the material is assumed to crush at that point. In concrete element, crushing is defined as the complete deterioration of the structural integrity of the material (e.g. material spalling). Under conditions where crushing has occurred, material strength is assumed to have degraded to an extent such that the contribution to the stiffness of an element at the integration point in question can be reduced or ignored.

Analysis procedure for nonlinear FEM model

Figure 2 shows the typical FRP confined rectangular concrete column and definitions of geometric dimension, where B = column width (longest side length); D = column depth (shortest side length); H = column height; r = corner radius and t_j = thickness of reinforcing FRP. For FRP confined rectangular concrete columns, the FRP volumetric ratio (ρ_j) is defined as:

$$\rho_j=\frac{V_{FRP}}{V_{concrete}}=\frac{H\,[2(B-2r)+2(D-2r)+2\pi r]\,t_j}{H(B\times D-4r^2+\pi r^2)}$$

$$=\frac{[2(N+1)(D/r)-(8-2\pi)]\,t_j}{[N(D/r)^2-(4-\pi)]\,r};\ where\ N=B/D \tag{9}$$

The element meshes of the nonlinear finite element model for FRP confined square concrete columns (B/D=1) with various column side to corner radius ratios (D/r) are shown in Figure 3.

In a square section, the stress fields are unequal in lateral direction, therefore the concrete must be divide into different materials $(f_c^m)_i$ classified by the smallest $(f_{l1})_i$ and the largest $(f_{l2})_i$ confining stresses. The

typical lateral confining stress and different material patterns are shown in Figure 4. The stress-strain characteristics of the confining mechanism are explicitly accounted for, while the lateral strain of concrete is implicitly obtained through the interactive procedure as shown in Figure 5. The analysis procedure for nonlinear FEM model consists of the following basic steps:

1.given axial strain $(\varepsilon_c)_i$ and different materials $(f_c^m)_{i-1}$ obtaining from previous step for step i;

2.from equations (1)~(4) to form nonlinear FEM model for square section confined concrete;

3.from nonlinear FEM model, find $(f_c)_i$, $(f_{l1})_i$, and $(f_{l2})_i$;

4.assign new materials $(f_c^m)_i$ classified by $(f_{l1})_i$, and $(f_{l2})_i$;

5.check $\begin{cases} concrete\ failure\ occurence\ by\ Willam's\ criterion \\ composite\ failure\ occurence\ by\ \varepsilon_l \geq \varepsilon_{ju}\ or\ f_l \geq f_{ju} \end{cases}$;

6.next *i*.

EXPERIMEMTAL PROGRAM

Preparation of CFRP confined concrete specimens

A total of 28 concrete columns with different dimension were constructed and tested under axial compression. The main experimental parameters include column size, CFRP volumetric ratio, column side to corner radius ratio and column side aspect ratio. Table 1 summarized the test matrix. Dimensions of the column size (*D*) considered are 15, 30 and 45 cm. The CFRP volumetric ratios are 0.5 and 1.0%. The column side to corner radius ratios (*D/r*) are 5, 10 and 15. The column side aspect ratios (*B/D*) are 1.0, 1.5 and 2.0.

The specimen preparation work can be divided into two stages: making rectangular concrete columns and hand layout the CFRP around these columns. The hand layout procedures are described as follows. A thin layer of primer epoxy was first applied to the concrete surface. After the primer epoxy on concrete surface was cured at the ambient temperature for several hours, the carbon fiber sheet was applied to the concrete columns. For installing the sheet and the other on top of the installed sheet, were applied using paintbrush or rollers to fully saturate the carbon fiber with epoxy. The extra epoxy for each layer was squeezed out using a flat plastic scraper. The length of overlay is more than 10 cm, and the duration of applying next layer should be more than one day. After the required sheet layers were applied, the CFRP jacketing was cured in the ambient condition.

Test method and test setup

As shown in Photo 1(a), all the specimens were tested using a high-stiffness, high-capacity (58800kN) compression testing machine at the Structural Laboratory of Lien-Foo pillar plastic Inc. This unique equipment has sufficient capacity and stiffness, require for conducting such tests. The machine is also equipped with a sophisticated computer control and data acquisition system, as shown in Photo 1(b) and Photo 1(c).

The test procedure was followed the ASTM C39 and CNS 1232 standard and the testing strain rate was 25 micro-strain/sec. The acquired data included the applied axial load, *P*, axial deformation of concrete, and transverse and axial strain of the FRP jacket. As shown in Photo 2, in order to obtain data without the influence due to the possible imperfect contacts as well as the end confinement due to the friction between the ends of the specimen and the loading platens, the axial deformation of the concrete was measured for the middle portion with a gauge length of *H/2*, using a special device and linear potentiometers. The jacket strains were measured using electrical resistance gauges with a gauge length 10mm.

Experimental results

Test results of FRP confined square concrete columns are shown in Table 3. For columns with the same CFRP volumetric ratio (0.5%), the compressive strength of square concrete columns decrease as the column side to corner radius ratio (*D/r*) increase, from 452.24 and 416.60 kgf/cm^2 to 307.57 and 297.75

kgf/cm^2. As the same, the ultimate axial strain of square concrete columns decrease as the column side to corner radius ratio (*D/r*) increase, from 1.89 and 1.56% to 1.31 and 1.33%.
Test results of FRP confined rectangular concrete columns are shown in Table 4. For columns with the same CFRP volumetric ratio (1.0%) and column side to corner radius ratio (*D/r*=10), the compressive strength of rectangular concrete columns decrease as the column side aspect ratio (*B/D*) increase, from 338.77 and 354.82 kgf/cm^2 to 317.52 and 293.53 kgf/cm^2. As the same, the ultimate axial strain of rectangular concrete columns decrease as the column side aspect ratio (*B/D*) increase, from 1.52 and 1.56% to 1.43%.
Detail comparison between experimental results and analysis results are shown in next section.

COMPARISON WITH EXPERIMENTAL RESULTS

Tests by Rochette et al., 2000 [6]
Tests were carried out on thirteen 500-mm-high concrete specimens with square section. They had 152×152 mm sides with different corner radii and were wrapped by either three, four, or five carbon plies. The mechanical properties of the composites were E_j = 82.7GPa, ε_{ult} = 1.5%, t_j = 0.30 mm, and w = 1.8 g/cm^3. The unconfined concrete properties were f'_{co} = 42.0MPa, ε_{co} = 0.002, E_c = 32,400MPa, and ν = 0.2.
Table 2 lists the experimental results and those obtained from the nonlinear FEM analyses. The results show that the errors of normalized compressive strengths for proposed models are -0.17, 1.41, 4.46, and 8.61% corresponding to specimens C100-C2, S38-C3, S25-C3 and S5-C3, respectively. Also, the results show that the errors of ultimate axial strains for the proposed models are -2.67, 0.34, 0.90, and -4.05% for the same specimens. Figure 6 shows the comparisons between tests and analyses for the axial stress versus axial strain. As it can be seen in Table 2 and Figure 6, the agreement between nonlinear finite element results (solid lines) and experimental results (markers) is very satisfactory.

Tests by present study
Table 3 and 4 lists the experimental results and those obtained from the nonlinear FEM analyses. The results show that the errors of normalized compressive strengths for proposed models are small than 9.61%, expect for specimens S15-DR05-C2-200-2 and S30-DR10-C3-250-1. Also, the results show that the errors of ultimate axial strains for the proposed models are small than 8.98%, expect for specimens S15-DR05-C2-200-2, S30-DR10-C3-250-1, R15-BD1.5-DR05-C2-250-2 and R15-BD2.0-DR05-C4-250-2.
The comparison between experimental results and nonlinear finite element analysis results are shown in Figure 7 to Figure 11. The detail of comparison is described as follows.

Effect of column side aspect ratio (B/D)
For the columns of fixed CFRP volumetric ratio (1.0%), the effect of column side aspect ratio (*B/D*) to the compressive strength and ultimate strain of the CFRP confined rectangular concrete columns are shown in Figure 7. As shown in Figure 7(a) and 7(b), for columns with the same side to corner radius ratio (*D/r*= 5, 10), the normalized compressive strength and ultimate axial strain decrease as the column side aspect ratio (*B/D*) increase. As it can be seen in Figure 7, the agreement between nonlinear finite element results (solid lines) and experimental results (markers) is very satisfactory.

Effect of column side to corner radius ratio (D/r)
For the columns of fixed CFRP volumetric ratio (0.5 and 1.0%), the effect of column side to corner radius ratio (*D/r*) to the compressive strength and ultimate strain of the CFRP confined square concrete columns are shown in Figure 8. As shown in Figure 8(a) and 8(b), the normalized compressive strength and ultimate axial strain decrease as the column side to corner radius ratio (*D/r*) increase. As it can be seen in

Figure 8, the agreement between nonlinear finite element results (solid lines) and experimental results (markers) is very satisfactory.

Effect of CFRP volumetric ratio

For the columns of fixed column side to corner radius ratio (*D/r*= 5, 10 and 15), the effect of CFRP volumetric ratio to the compressive strength and ultimate strain of confined square concrete columns are shown in Figure 9. As shown in Figure 9(a) and 9(b), for columns with the same side to corner radius ratio (*D/r*= 5, 10 and 15), the normalized compressive strength and ultimate axial strain increase as the CFRP volumetric ratio increase. As it can be seen in Figure 9, the agreement between nonlinear finite element results (solid lines) and experimental results (markers) is very satisfactory.

Effect of column size (D)

For the columns of fixed CFRP volumetric ratio (1.0%), the effects of column size (*D*) to the compressive strength and ultimate axial strain of the CFRP confined rectangular concrete columns are shown in Figure 10 and 11. As shown in Figure 10 and 11, for columns with the same corner radius (*r*=3), the normalized compressive strength and ultimate axial strain decrease with increasing column size. Nevertheless, there are no size effects in normalized compressive strength and ultimate axial strain for columns with the same CFRP volumetric ratio and column side to corner radius ratio (*D/r*). As it can be seen in Figure 10 and 11, the agreement between nonlinear finite element results (solid lines) and experimental results (markers) is very satisfactory.

PARAMETRIC STUDY

The parametric study is focused on three factors. They are the column size, reinforcing CFRP volumetric ratio and column side to corner radius ratio (*D/r*). Ranges of the column side length considered are from 20 cm to 200 cm, CFRP volumetric ratio from 0.0 to 3.0%, and column side to corner radius ratio from 2 to 60, while keeping the plain concrete strength to 27.47MPa (280 kgf/cm^2). The CFRP properties are E_j = 230.54GPa, f_{ju} = 1,152.67MPa, ε_{ju} = 0.005, and t_j = 0.1375mm/layer (FAW 250).

Effect of column side aspect ratio (*B/D*)

For the columns of fixed plain concrete strength (27.47Mpa) and column side to corner radius ratio (*D/r*=10), the influence of changing the column side aspect ratio (*B/D*) to the compressive strength and ultimate strain of the CFRP confined rectangular concrete columns is studied. Results of parametric study are shown in Figure 12. As shown in Figure 12(a), for columns with the same CFRP volumetric ratio (0.1, 0.5, 1.0, 2.0, and 3.0%), the normalized compressive strength of rectangular concrete columns decrease rapidly as the column side aspect ratio (*B/D*) increase. As the same, the ultimate axial strain of rectangular concrete columns decrease as the column side aspect ratio (*B/D*) increase, shown in Figure 12(b).

Effect of column side to corner radius ratio (*D/r*)

For the columns of fixed plain concrete strength (27.47MPa) and column side aspect ratio (*B/D*=1), the influence of changing the column side to corner radius (*D/r*) to the compressive strength and ultimate strain of the CFRP confined square concrete columns is studied. Results of parametric study are shown in Figure 13. As shown in Figure 13(a), for columns with the same CFRP volumetric ratio (0.1, 0.5, 1.0, 2.0, and 3.0%), the normalized compressive strength of square concrete columns decrease rapidly as the column side to corner radius ratio increase. As the same, the ultimate axial strain of square concrete columns decrease as the column side to corner radius ratio (*D/r*) increase, shown in Figure 13(b).

Effect of CFRP volumetric ratio (ρ_j)

For the columns of fixed plain concrete strength (27.47MPa) and column side aspect ratio (*B/D*=1), the influence of changing the CFRP volumetric ratio (ρ_j) to the compressive strength and ultimate strain of the CFRP confined square concrete columns is studied. Results of parametric study are shown in Figure 14. As shown in Figure 14(a), for columns with the same column side to corner radius ratio (*D/r*=2, 4, 10, 20 and 30), the normalized compressive strength of square concrete columns increase as the CFRP volumetric ratio increase. As the same, the ultimate axial strain of square concrete columns increase as the CFRP volumetric ratio increase, shown in Figure 14(b).

Effect of column size (*D*)

For the columns of equal plain concrete strength (27.47MPa) and column side aspect ratio (*B/D*=1), the influence of changing the column size to the compressive strength and ultimate axial strain of the CFRP confined square concrete columns is studied. Results of the parametric study are shown in Figure 15. As shown in Figure 15(a), for columns with the same corner radius (*r*=3, 5 and 10) and CFRP volumetric ratio (0.5 and 3.0%), the normalized compressive strength of square concrete columns decrease with increasing column size. Nevertheless, there are no size effects in normalized compressive strength for columns with the same CFRP volumetric ratio and column side to corner radius ratio (*D/r*). Similarly, as shown in Figure 15(b), for columns with the same corner radius and CFRP volumetric ratio, the ductility (ultimate axial strain) of square concrete columns decrease with increasing column size. Nevertheless, there are no size effects in ductility for columns with the same CFRP volumetric ratio and column side to corner radius ratio (*D/r*).

CONCLUDING REMARKS

For the effects of change column size (*D*), CFRP volumetric ratio (ρ_j), column side to corner radius ratio (*D/r*) and column side aspect ratio (*B/D*) to strength and ductility of CFRP confined rectangular concrete columns. It is imperative that:
(1) the normalized column axial strength and ductility increase with increasing CFRP volumetric ratio, but decrease with increasing column side to corner radius ratio (*D/r*) and column side aspect ratio (*B/D*), (2) for columns with the same corner radius and CFRP volumetric ratio, the normalized column axial strength and ductility decrease with increasing column size (*D*) and (3) there are no size effects on normalized strength and ductility for columns with the same CFRP volumetric ratio, column side to corner radius ratio (*D/r*) and column side aspect ratio (*B/D*).

ACKNOWLEDGEMENTS

Results of this study are supported by grants from the National Science Council (NSC 89-2625-Z-002-067)

REFERENCES

1. Kupfer, H., H.K. Hilsdrof, and H. Rusch (1969), “Behavior of Concrete under Biaxial stresses”, Journal of American Concrete Institute, 66, 656-666.
2. Mander, J.B., M.J.N. Priestley, and R. Park (1988), “Theoretical Stress Strain Model for Confined Concrete,” Journal of Structural Engineering, ASCE, 114(8), 1804-1826.
3. Chang, G.A., and J.B. Mander (1994), “Seismic Energy Based Fatigue Damage Analysis of Bridge Columns: Part I – Evaluation of Seismic Capacity”, Technical Report NCEER-94-0006, NCEER, State University of New York, Buffalo, N.Y., 3-32 – 3-34.

4. Chang, K.C., and F.Y. Yeh (2002), "Effect of Size and Strength on FRP Confinements for Circular Concrete Columns", Taiwan-Canada Workshop on Bridges, April, 2002, Taipei, Taiwan, 27-38.
5. Willam, K. J., and E. P. Warnke (1975). "Constitutive Model for the Triaxial Behavior of Concrete", Int. Assoc. Bridge Struct. Eng. Sem. Concr. Struct. Subjected Triaxial Stresses, Bergamo, Italy, 1974, Int. Assoc. Bridge Struct. Eng. Proc., 19, 1-30.
6. Rochette, P., and P. Labossiere (2000), "Axial Testing of Rectangular Column Models Confined with Composites," Journal of Composites for Construction, 4(3), 129-136.

Table 1. The experimental parameters of 28 FRP confined concrete columns

Specimen No.	Concrete strength $f_{co}^{'}$	Column width B	Side length D	Column height H	Corner radius r	Number of layer	FRP type FAW	FRP volumetric ratio ρ_j	amount N
	kgf/cm^2	cm	cm	cm	cm		g/m^2	%	set
S15-DR05-C2-200	210	15	15	30	3	2	200	0.56%	2
S15-DR05-C3-250	210	15	15	30	3	3	250	1.04%	2
S30-DR10-C3-250	210	30	30	60	3	3	250	0.53%	2
S30-DR10-C5-300	210	30	30	60	3	5	300	1.06%	2
S45-DR15-C4-300	210	45	45	90	3	4	300	0.57%	2
S45-DR15-C7-300	210	45	45	90	3	7	300	1.00%	2
R15-BD1.5-DR05-C2-250	210	22.5	15	45	3	2	250	0.58%	2
R15-BD1.5-DR05-C3-300	210	22.5	15	45	3	3	300	1.05%	2
R30-BD1.5-DR10-C3-300	210	45	30	90	3	3	300	0.53%	2
R30-BD1.5-DR10-C6-300	210	45	30	90	3	6	300	1.07%	2
R15-BD2.0-DR05-C2-250	210	30	15	60	3	2	250	0.53%	2
R15-BD2.0-DR05-C4-250	210	30	15	60	3	4	250	1.06%	2
R30-BD2.0-DR10-C4-250	210	60	30	120	3	4	250	0.54%	2
R30-BD2.0-DR10-C8-250	210	60	30	120	3	8	250	1.07%	2

Table 2. Comparisons between tests (Rochette et al., 2000) and results of nonlinear finite element model for FRP confined square concrete columns

Specimen	Dimension (mm)	$f_{cc}^{'}/f_{co}^{'}$ (MPa) (Experiment)	$f_{cc}^{'}/f_{co}^{'}$ (MPa) (NFEM)	Error (%)	ε_{cu} (%) (Experiment)	ε_{cu} (%) (NFEM)	Error (%)
C100-C2	152 × 152	1.75	1.747	-0.17	1.57	1.528	-2.67
S38-C3	152 × 152	1.20	1.217	1.41	1.16	1.164	0.34
S25-C3	152 × 152	1.03	1.076	4.46	0.89	0.898	0.90
S5-C3	152 × 152	0.94	1.021	8.61	0.69	0.662	-4.05

Table 3. The error analysis of FRP confined square concrete columns between nonlinear finite element model and experimental results

Specimen No.	Dimension (mm)	ρ_j (%)	$f_{cc}^{'}$ (kgf/cm^2)	$f_{cc}^{'}/f_{co}^{'}$ (Exp.)	$f_{cc}^{'}/f_{co}^{'}$ (NFEM)	Error (%)	ε_{cu} (%) (Exp.)	ε_{cu} (%) (NFEM)	Error (%)
S15-DR05-C2-200-1	150×150×300	0.56	452.24	2.15	2.19	1.89	1.89	1.92	1.48
S15-DR05-C2-200-2	150×150×300	0.56	416.60	1.98	2.19	10.61	1.56	1.92	23.09
S15-DR05-C3-250-1	150×150×300	1.04	568.62	2.71	2.88	6.52	2.33	2.35	0.85
S15-DR05-C3-250-2	150×150×300	1.04	581.35	2.77	2.88	4.18	2.30	2.35	2.02
S30-DR10-C3-250-1	300×300×600	0.53	321.69	1.53	1.71	11.36	1.20	1.49	24.24
S30-DR10-C3-250-2	300×300×600	0.53	343.75	1.64	1.71	4.21	1.53	1.49	-3.04
S30-DR10-C5-300-1	300×300×600	1.06	436.69	2.08	2.18	4.65	1.78	1.81	1.72
S30-DR10-C5-300-2	300×300×600	1.06	416.94	1.99	2.18	9.61	1.91	1.81	-5.58
S45-DR15-C4-300-1	450×450×900	0.57	307.57	1.46	1.52	3.77	1.31	1.35	2.54

S45-DR15-C4-300-2	450×450×900	0.57	297.75	1.42	1.52	7.19	1.33	1.35	1.29
S45-DR15-C7-300-1	450×450×900	1.00	349.84	1.67	1.80	8.08	1.53	1.55	1.66
S45-DR15-C7-300-2	450×450×900	1.00	371.60	1.77	1.80	1.75	1.60	1.55	-3.26

Table 4. The error analysis of FRP confined rectangular concrete columns between nonlinear finite element model and experimental results

Specimen No.	Dimension (mm)	ρ_j (%)	$f_{cc}^{'}$ (kgf/cm^2)	$f_{cc}^{'}/f_{co}^{'}$ (Exp.)	$f_{cc}^{'}/f_{co}^{'}$ (NFEM)	Error (%)	ε_{cu} (%) (Exp.)	ε_{cu} (%) (NFEM)	Error (%)
R15-BD1.5-DR05-C2-250-1	150×225×450	0.58	374.74	1.78	1.83	2.53	1.65	1.69	2.21
R15-BD1.5-DR05-C2-250-2	150×225×450	0.58	357.69	1.70	1.83	7.41	1.22	1.69	38.37
R15-BD1.5-DR05-C3-300-1	150×225×450	1.05	460.19	2.19	2.22	1.35	1.94	2.02	4.01
R15-BD1.5-DR05-C3-300-2	150×225×450	1.05	454.47	2.16	2.22	2.63	2.00	2.02	0.90
R30-BD1.5-DR10-C3-300-1	300×450×900	0.53	301.19	1.43	1.45	0.89	1.31	1.33	1.43
R30-BD1.5-DR10-C3-300-2	300×450×900	0.53	290.30	1.38	1.45	4.67	1.37	1.33	-3.39
R30-BD1.5-DR10-C6-300-1	300×450×900	1.07	338.77	1.61	1.72	6.44	1.52	1.58	4.41
R30-BD1.5-DR10-C6-300-2	300×450×900	1.07	354.82	1.69	1.72	1.62	1.56	1.58	1.39
R15-BD2.0-DR05-C2-250-1	150×300×600	0.53	327.73	1.56	1.60	2.52	1.47	1.50	1.79
R15-BD2.0-DR05-C2-250-2	150×300×600	0.53	321.79	1.53	1.60	4.42	1.43	1.50	5.04
R15-BD2.0-DR05-C4-250-1	150×300×600	1.06	375.78	1.79	1.93	7.74	1.52	1.82	20.16
R15-BD2.0-DR05-C4-250-2	150×300×600	1.06	365.61	1.74	1.93	10.74	1.76	1.82	3.64
R30-BD2.0-DR10-C4-250-1	300×600×1200	0.54	275.12	1.31	1.33	1.19	1.20	1.24	3.43
R30-BD2.0-DR10-C4-250-2	300×600×1200	0.54	259.12	1.23	1.33	7.44	1.26	1.24	-1.69
R30-BD2.0-DR10-C8-250-1	300×600×1200	1.07	317.52	1.51	1.52	0.60	1.43	1.45	1.27
R30-BD2.0-DR10-C8-250-2	300×600×1200	1.07	293.53	1.40	1.52	8.82	1.60	1.45	-8.98

(a) (b) (c)

Photo 1. Compression testing machine at Lien-Foo pillar plastic Inc. (a) high-capacity testing machine, (b) computer control system, and (c) data acquisition system

(a) (b)

Photo 2. Test and instrumentation configurations, (a) square columns and (b) rectangular columns

(c) (d)

Photo 3. Typical example of failure mechanism, (a) FRP failure mode and (b) concrete failure mode

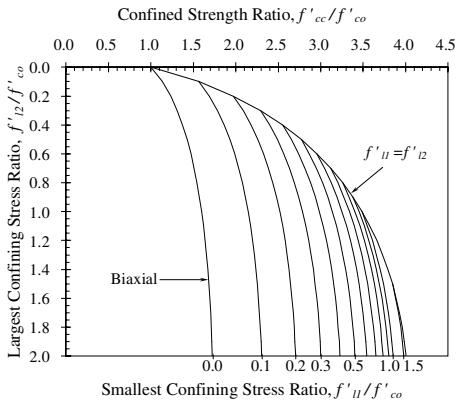

Fig.1. Confined strength determination from lateral confining stresses for square and rectangular sections

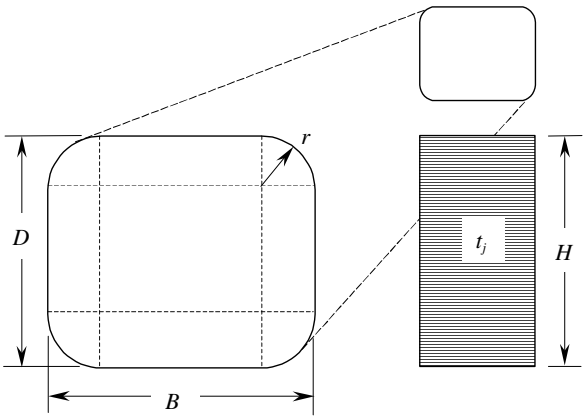

Fig.2. Definitions of geometric dimension for FRP confined rectangular concrete columns

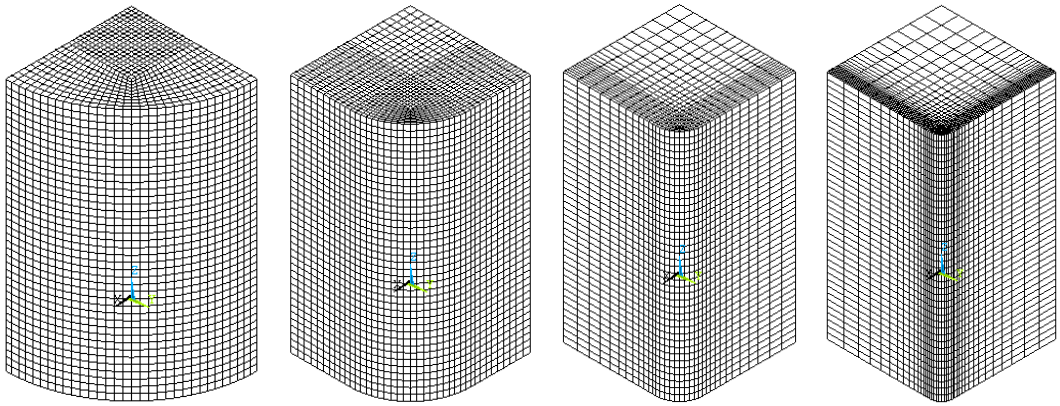

(a) (b) (c) (d)

Fig.3. Element mesh of nonlinear FEM model for FRP confined square concrete columns (B/D = 1) with different column side to corner radius ratio (a) D/r = 2, (b) D/r = 4, (c) D/r = 10, and (d) D/r = 20

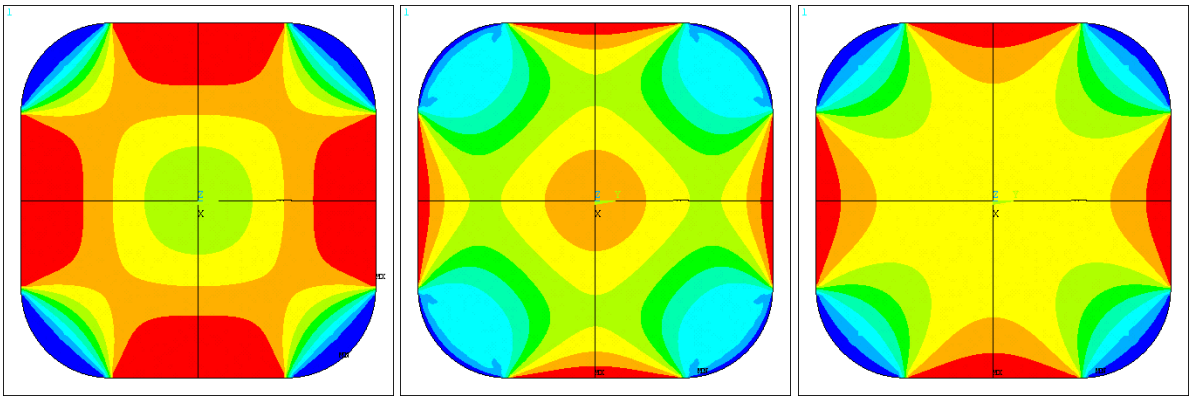

(a) (b) (c)

Fig.4 Characteristic of FRP confined square concrete columns (a) smallest confining stress $(f_{l1})_i$, (b) largest confining stress $(f_{l2})_i$, and (c) $(f_c^m)_i$ for different concrete material classified by $(f_{l1})_i$ and $(f_{l2})_i$

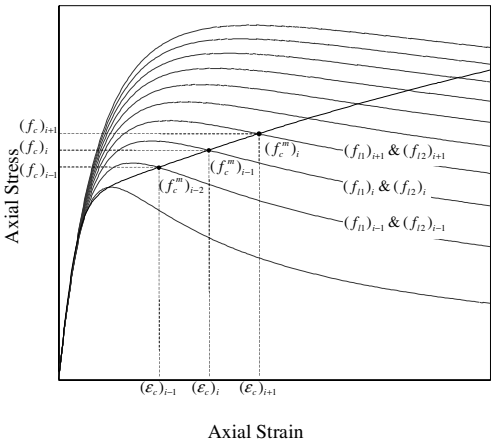

Fig.5. Nonlinear finite element analysis procedure for FRP confined square concrete columns

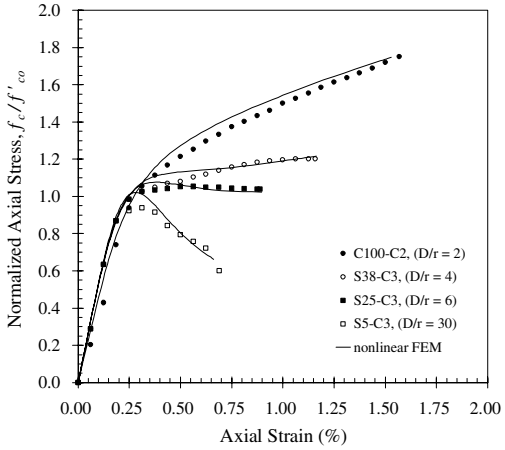

Fig.6. Comparisons between tests (Rochette et al. 2000) and analyses for axial stress versus axial strain

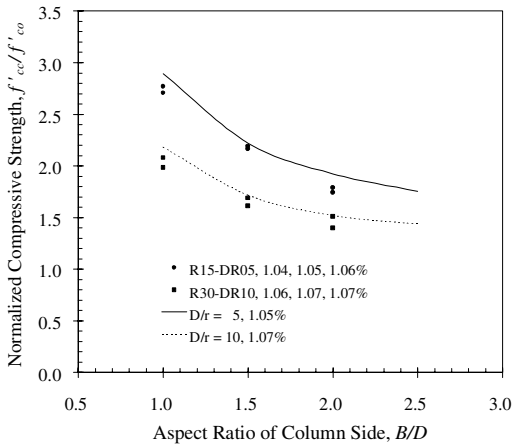

(a)

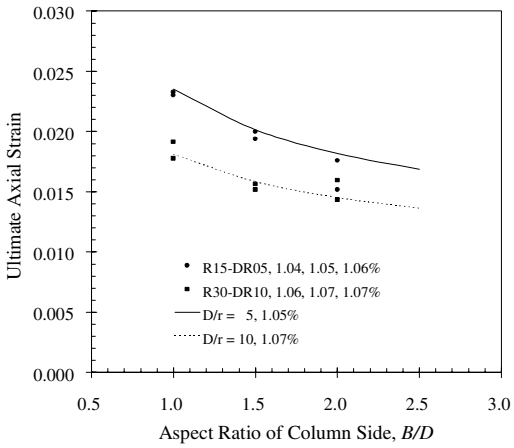

(b)

Fig.7. Comparisons for effect of column side aspect ratio (*B/D*) on (a) normalized compressive strength and (b) ultimate axial strain between experiment and analysis results for columns with ρ_j = 1.05%

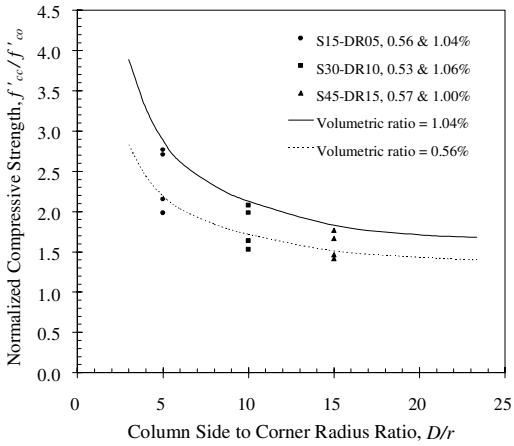

(a)

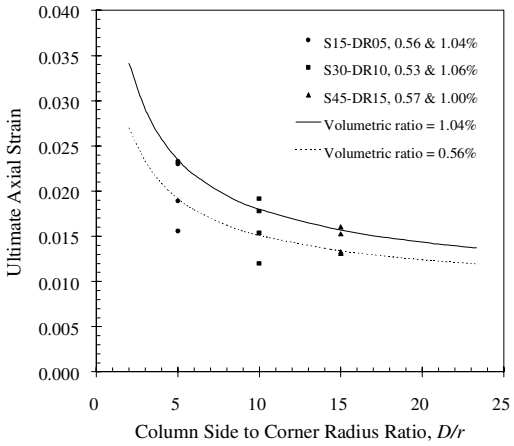

(b)

Fig.8. Comparisons for effect of column side to corner radius ratio (*D/r*) on (a) normalized compressive strength and (b) ultimate axial strain between experiment and analysis results for columns with *B/D* = 1

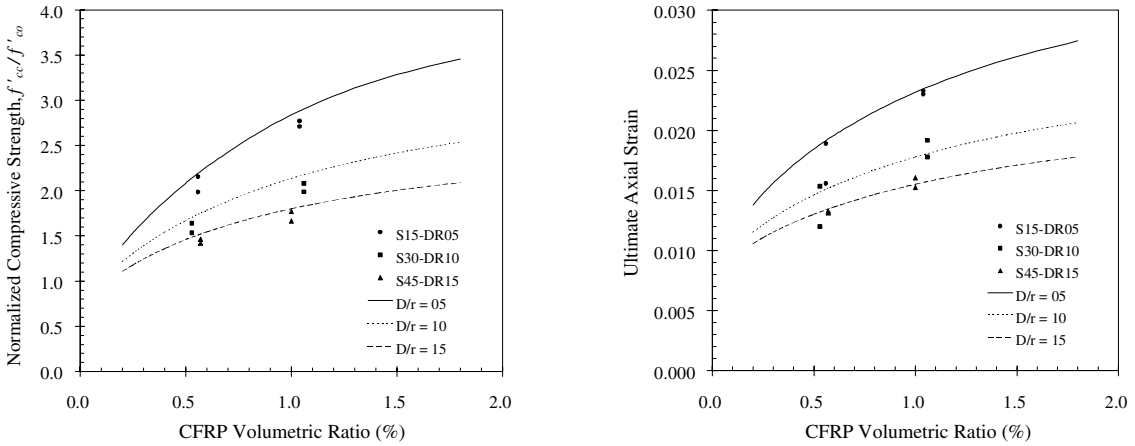

(a) (b)

Fig.9. Comparisons for effect of CFRP volumetric ratio (ρ_j) on (a) normalized compressive strength and (b) ultimate axial strain between experiment and analysis results for columns with *B/D* = 1

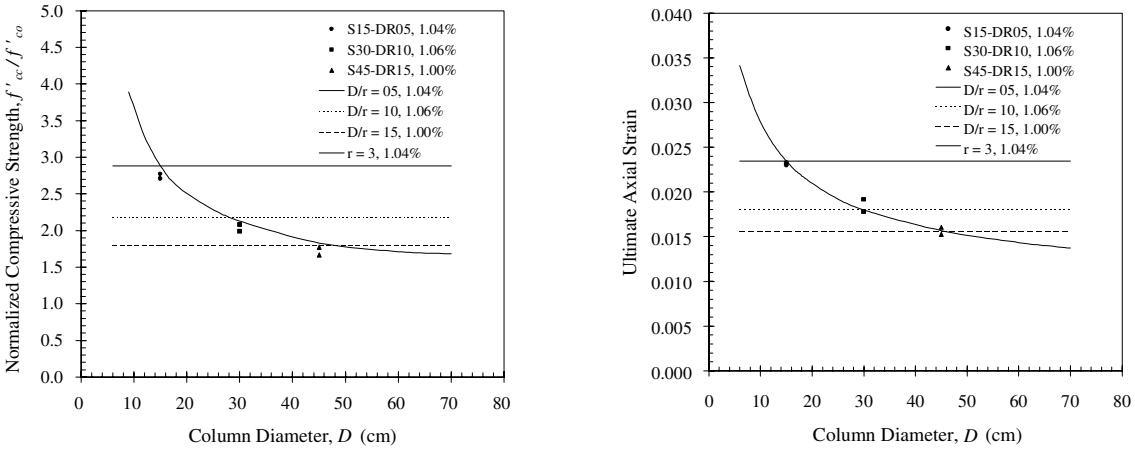

(a) (b)

Fig.10. Comparisons for effect of column size (*D*) on (a) normalized compressive strength and (b) ultimate axial strain between experiment and analysis results for columns with *B/D* = 1 and ρ_j = 1.05%

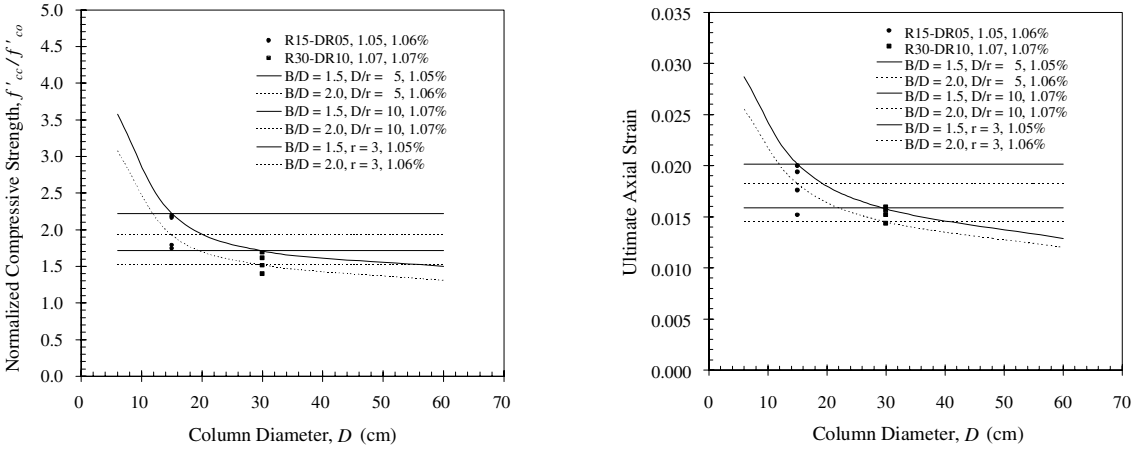

(a) (b)

Fig.11. Comparisons for effect of column size (*D*) on (a) normalized compressive strength and (b) ultimate axial strain between experiment and analysis results for columns with ρ_j = 1.05%

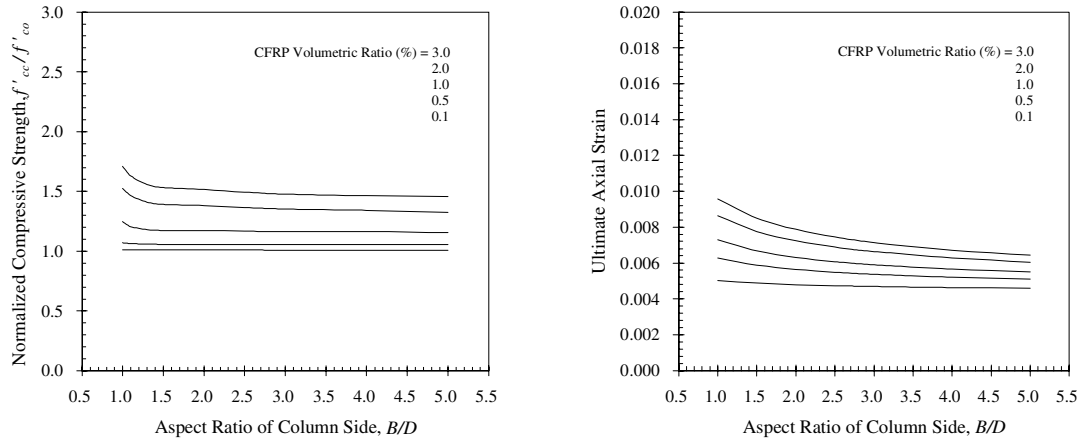

(a) (b)

Fig.12. Effect of column side aspect ratio (*B/D*) on (a) normalized compressive strength and (b) ultimate axial strain for columns with *D/r* = 10 and f'_{co} = 27.47MPa

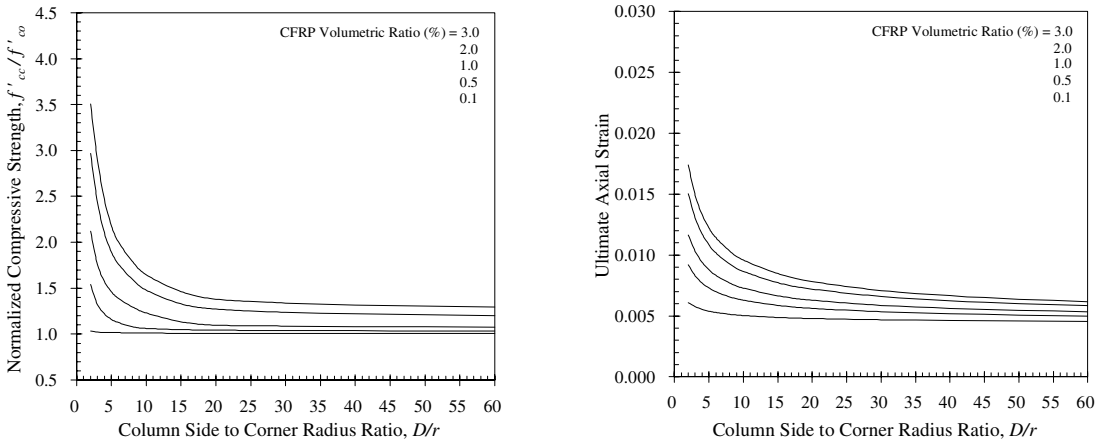

(a) (b)

Fig.13. Effect of column side to corner radius ratio (*D/r*) on (a) normalized compressive strength and (b) ultimate axial strain for columns with *B/D* = 1 and f'_{co} = 27.47MPa

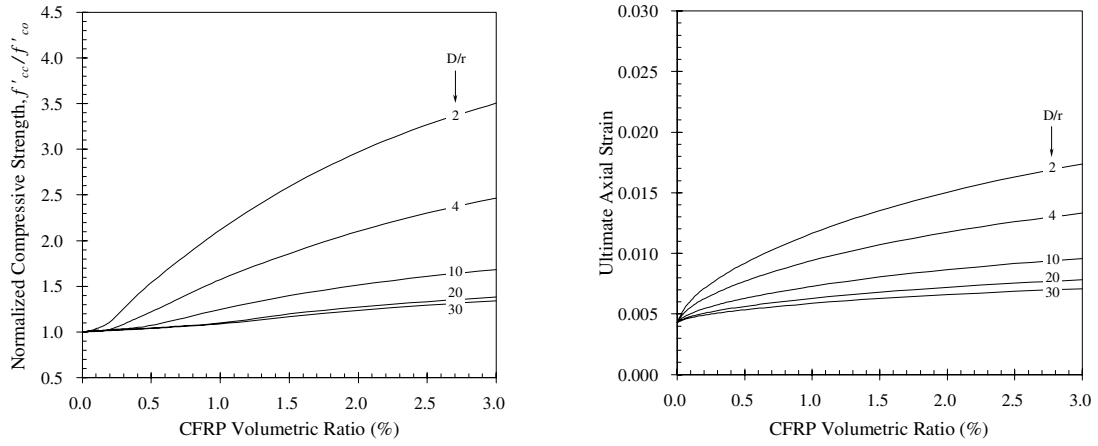

(a) (b)

Fig.14. Effect of CFRP volumetric ratio (ρ_j) on (a) normalized compressive strength and (b) ultimate axial strain for columns with *B/D* = 1 and f'_{co} = 27.47MPa

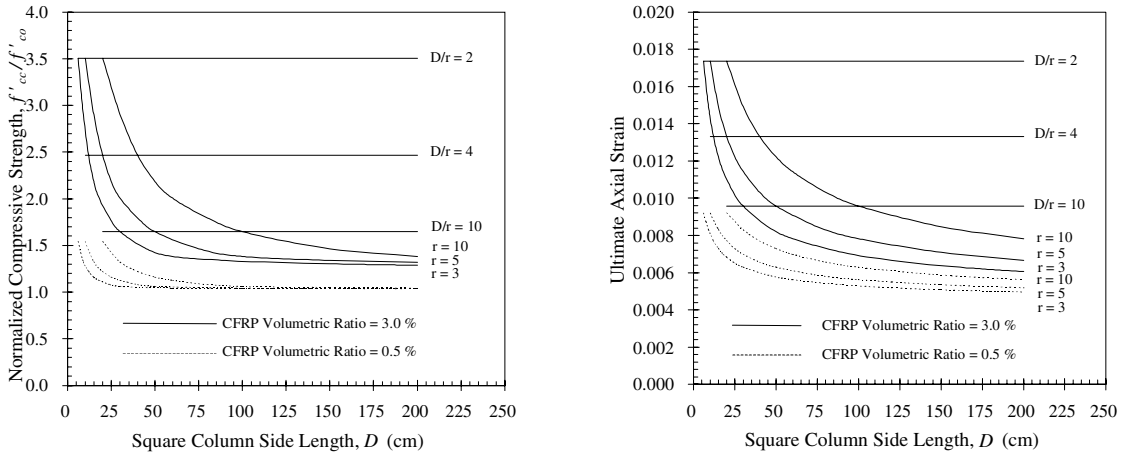

(a) (b)

Fig.15. Effect of column size (D) on (a) normalized compressive strength and (b) ultimate axial strain for columns with B/D = 1 and f'_{co} = 27.47MPa